Hindawi
Wireless Communications and Mobile Computing
Volume 2022, Article ID 6904653, 12 pages
https://doi.org/10.1155/2022/6904653

Research Article

Interactive Multimedia Data Coscattering Point Imaging for Low Signal-to-Noise Ratio 3D Seismic Data Processing

Jianbo Fei and Yanchun Wang

School of Geophysics and Information Technology, China University of Geosciences, Beijing 100083, China

Correspondence should be addressed to Jianbo Fei; 3010190018@cugb.edu.cn

Received 30 May 2022; Revised 14 July 2022; Accepted 22 July 2022; Published 4 August 2022

Academic Editor: Jun Ye

In this paper, low signal-to-noise ratio 3D seismic data are processed by the method of coscattered point imaging, and the imaging method is analyzed in combination with interactive multimedia for 3D seismic data. The reconstruction is carried out using a convex set projection algorithm based on the curvilinear wave transform. The track set is extracted from the 3D data body and transformed into the common offset distance-center point tract set to achieve the reconstruction of seismic data in the common offset distance track set domain and through comparison. It is concluded that the reconstruction effect is better in the common. The reconstruction results are better in the common offset distance track set domain. To shorten the processing time and obtain better reconstruction results, this paper proposes the idea of direct reconstruction of frequency slices. Experiments on the actual seismic three-component wavefield based on velocity-type and acceleration-type three-component geophones are carried out to reveal the signal characteristics of the actual seismic wavefield under the mining space. Due to the limitation of the construction observation space and the particularity of the actual needs of mine detection, the application of the scattered wave imaging method in the mine must be based on the corresponding detection space and detection purpose. The implementation of this thesis improves the signal-to-noise ratio, resolution, and fidelity of the 3D seismic data of the Shawan Formation, which is more conducive to the search for lithological traps. Combined with the seismic geological data, several traps were finally found and implemented, indicating that the fidelity of the resultant information is good and can meet the needs of interpretation and comprehensive research. The multiwave scattering imaging method in this paper can complete multiwave field imaging of longitudinal, transverse, and slot waves, which has the advantages of data redundancy, high superposition number, and more accurate imaging than conventional reflection wave imaging and provides field application value for ensuring mine safety production.

1. Introduction

Seismic signal noise suppression to improve the signal-to-noise ratio is the primary task of seismic data processing. Because seismic signals are affected by complex geological structures and surface environment, exploration instrument interference, and other unavoidable environmental factors, the acquired seismic signals contain random noise and regular noise. Random noise has a wide frequency and no fixed propagation direction; regular noise is also equivalent to coherent noise [1]. Coherent noise contains surface waves, multiple waves, refractive waves, acoustic waves, and other noise with certain dynamics, which have regular main frequencies and apparent velocities and are relatively easy to distinguish. The nature of the noise is different, and the suitable denoising methods are different. There are differences in frequency and apparent velocity between effective seismic waves and coherent noise, so coherent noise can be removed by one-dimensional frequency filtering and two-dimensional apparent velocity filtering [2]. With the rapid advancement of computer technology, seismic data processing can also fully rely on advanced processing technology, which requires not only the resolution and fidelity to be guaranteed but also the processing efficiency to be improved to a great extent to adapt to the complexity and difficulty of exploration work. Processing the acquired large-scale data and displaying them visually

using computer graphics and imaging to achieve convenient human-computer interaction provide an effective technical means for the technical personnel at the exploration site to observe and interpret the data [3]. It is also a very large part of the workload invested by researchers in seismic data processing.

The surface observation seismic profile is to excite seismic waves at some points near the surface and at the same time to observe at some points arranged along the surface measurement line; the vertical seismic profile is also to excite seismic waves at some points near the surface, but it is to observe at some points arranged at different depths along the borehole [4]. The former geophone is placed on the surface, and the measurement line is arranged along the ground, so it is also called a horizontal (or ground) geophone profile; the latter geophone is placed in the well, and the measurement line is arranged vertically along the wellbore, so it is called vertical geophone profile. In the horizontal seismic profile, because the geophone is placed on the ground, only upward waves from the subsurface can be received in addition to the direct and surface waves propagating along the surface; in the vertical seismic profile, because the geophone is placed inside the formation through the well, both upward and downward waves propagating from the bottom can be received. In the field of geological exploration, before the emergence of three-dimensional visualization technology, researchers often obtain geological information through cross-sectional images [5]. This method of interpreting three-dimensional information by two-dimensional means has great limitations, making it difficult to grasp the underground structure, resulting in most of the data being wasted and low utilization of resources. Records are presented as half-branch of the hyperbola. As the CSP gather deviates from the scattering point, the equivalent offset of the effective scattered wave increases, and the small equivalent offset signal lacks data and appears as a hyperbolic far-branch signal in morphology. The 3D visualization of seismic data can provide geologists with a visual reference of the geological structure and geological model, and it can help to reveal the intrinsic laws of geological data, which can lead to activities such as energy exploration and thus generate great economic benefits.

The experiments on the actual three-component wavefield of mine seismic based on velocity-type and acceleration-type three-component geophones were carried out to reveal the signal characteristics of the actual seismic wavefield under the mining space by analyzing the differential characteristics of the coal seismic waves in the time-frequency domain and polarization parameters, to evaluate the field applicability of the two types of geophones, and to provide application guidance for mine seismic exploration.

2. Related Works

Among the data visualization methods, the research of 2D visualization algorithms started earlier, and there are many mature 2D visualization software. As the visualization research progressed, researchers began to favor 3D visualization methods with higher data utilization, trying to find better 3D visualization and use its richer expressive power to overcome some limitations of 2D visualization [6]. At present, the purpose of 3D visualization of seismic data is to reflect the inline information between data more efficiently to improve the accuracy of oil and gas exploration and accelerate the exploration process, rather than pursuing more detailed and realistic 3D scenes; however, due to the increasingly large amount of 3D seismic data obtained by advanced data acquisition techniques, although the emergence of GPU has eased the pressure of CPU in processing 3D geometric operations, GPU is also limited by the size of memory and cannot directly cope with the massive data exceeding the memory scale, so it is difficult to load the data completely into the memory and then process it in the process of data visualization and other applications [7]. The traditional body data rendering process is exactly loading the body data completely into memory at one time, and the rendering module only gets the data from memory, so this approach fails for large seismic data that exceeds the memory scale [8].

Bakulin et al. proposed a wavefront method for interpreting seismic refraction waves, i.e., using Huygens' principle to reconstruct the wavefront field based on the recorded first-to-wave travel time at two gun sites, and then calculate the depth of the refraction layer based on the velocity above the refraction layer, but when the stratigraphy changes drastically, the circular wavefront theory does not match the actual situation and cannot be applied to this geological condition [9]. Shiraishi et al. proposed the delay time method to identify the refraction layer by calculating the relationship between the reciprocal time and the intercept time, but this method is limited in the imaging effect in subsurface formations with large dip angles and multiple media layers [10]. Schaaf and Bond further proposed the addition and subtraction method based on Thornburgh's wavefront method, in which the travel time of two-gun points to each geophone can be added to obtain [11]. This method calculates the exact value from the refractive layer to the surface through the "plus line" and "minus line." The generalized reciprocal method is a technique to image the undulating refractive layer at any depth based on the seismic refractive wave data consisting of forward and reverse travel times and to analyze the velocity of the refractive layer based on the travel times recorded by the geophone [12]. Using the upper cover velocity and refractive wave travel time data, the method can be used to calculate refractive layer images with higher resolution in complex near-surface structures [13].

Whether in the time domain or the frequency domain, the co-offset distance channel set seismic data reconstruction effect is the best with less loss of effective information. However, for the three-dimensional seismic data body, only one direction of information is utilized, and the reconstruction effect has a greater possibility of improvement. Therefore, two-dimensional random sampling is performed on the time slice of this data body, and the reconstruction process is the same as that of the above one-dimensional random undersampling missing seismic data, but the sampling data processed are the common gunpoint-checkpoint direction and the common offset distance-center point direction. The reconstruction accuracy of the reconstruction results is

significantly improved compared with the 1D random undersampling reconnection results. However, the reconstruction results of the common offset distance-center point under two-dimensional random sampling are not much better than the reconstruction results of the common gunpoint-checkpoint channel set, because the slope of the homophase axis of the reflected wave in the center point channel set is larger and the wave field is more complicated when the two directions are sampled.

3. Interactive Multimedia Data Coscattering Point Imaging Design

At present, mine seismic mainly serves to solve the problems of mine full-space hazard source detection and anomalous structure imaging accuracy, and the lithology of the actual mine site is usually known, so the subsequent study in this paper is carried out from simple to complex, using the uniform isotropic medium as the background. Due to the limitation of the construction observation space and the specificity of the actual demand for mine detection, the application of the scattered wave imaging method in mines must be based on the corresponding detection space and detection purpose, so the study of the mapping method for the set of scattered wave coscattered point paths in different typical detection modes is essential [14]. The purpose of utilizing the scattered wave signal in the transmission recording cannot be achieved. In the process of transforming the transmitted wave of the working face, all other possible travel time compensation methods were tried, but this fundamental problem could not be avoided. On this basis, scattered wave imaging and multiwave multicomponent methods can be integrated into the field of mine seismic to form a practical multiwave scattering imaging method for mines and make theoretical and application innovations.

The model is shown in Figure 1. The background velocity of the model is 3000 m/s, the scattering point velocity is 2000 m/s, the detection point is arranged at $X = 0{\sim}50$ m, $Z = 0$ m, the single gunpoint is arranged at $X = 50$ m, $Z = 0$ m, the channel spacing is 2.5 m, and the scattering point is located at $X = 100$ m, $Z = 0$ m.

The virtual survey line is established at $X = 50$ m, and the virtual survey line is in the range of $Z = -50{\sim}50$ m, and the mapping parameters of the coscattering point channel set of the overdetection are the following: the maximum equivalent offset distance is 100 m, the equivalent offset distance interval is 2 m, and the CSP point interval is 2 m. This method can transform the linear reflection wave in front of the original record into a scattered wave with hyperbolic arrival characteristics and significantly increase the number of signal superpositions. Under this equivalent method, the CSP channel set only has the signal of one side of the equivalent offset distance, and the record is presented as the half branch of the hyperbola because the actual gun check positions are located on one side of the detection area. As the CSP channel set deviates from the scattering point, the equivalent offset distance of the effective scattered wave increases, and the signal of small equivalent offset distance is missing data, which appears as the distant branch signal of the hyperbola in morphology and causes difficulties in the judgment of the top point of the scattered wave [15]. The CSP channel set under this equivalent method may still have scattered waves that may cause imaging artifacts even when it is not at the scattering point position, cannot avoid the arc drawing phenomenon of the conventional oversurvey offset imaging, and cannot distinguish the real scattering point signal.

When the source-receiver point is in the alleyway on both sides of the working face, the essence is the conventional transmission wave method observation system at the working face, and the detection area is the area between the source and receiver points. Specifically, for a certain scattering point, the travel time and path of the scattered wave are dynamic and known during mapping, then for any sampling point signal in the records of different shot detection pairs, the corresponding polarization factor. According to Huygens' principle, transmitted waves also belong to the category of scattered waves, and scattered waves will be generated when the transmitted waves encounter scattering points during the propagation of transmitted waves. From this, it is obtained that the equivalent offset distance of the source-receiver point on the working face side of the double-aisle is dominantly given by

$$h_e = v_e\left(\frac{t}{2}\cdot\frac{t_0}{t_i} - t_0^2\right)^{1/2}. \tag{1}$$

Suppose the source point is in the track lane and the receiving point is in the belt lane, currently, due to the change of the propagation path of the scattered wave. We try to introduce a new propagation travel time t_{rv} according to the equivalent offset distance; t_{rv} is the travel time of the scattered wave from the receiving point R to the vertical virtual receiving point $R^{'}$ of the opposite lane so that the total travel time of the scattered wave from the source point S through the scattering point to the receiving point R:

$$t = \left[t_0^2 - \frac{h_s^2}{v_s^2}\right]^{1/2} - \left[(t_{rv} - t_0)^{1/2} - \frac{h_s^2}{v_s^2}\right]^{1/2}. \tag{2}$$

The travel times of the scattered waves at different depth scattering points under the concept of equivalent offset distance do not satisfy the hyperbolic relationship when the source and receiver points are located in the alleyways on both sides of the working face, and the purpose of using the scattered wave signals in the transmission record cannot be achieved. In the process of working surface transmission wave modification, various other possible travel time compensation methods were tried but could not circumvent this fundamental problem, which originated from the nature of the actual observation system. Although it is difficult to solve this problem with the current method, it will be an important research direction to use the new method to modify the transmission wave so that its time distance satisfies the hyperbolic relationship, which in turn satisfies the conventional seismic processing method, greatly improves the data

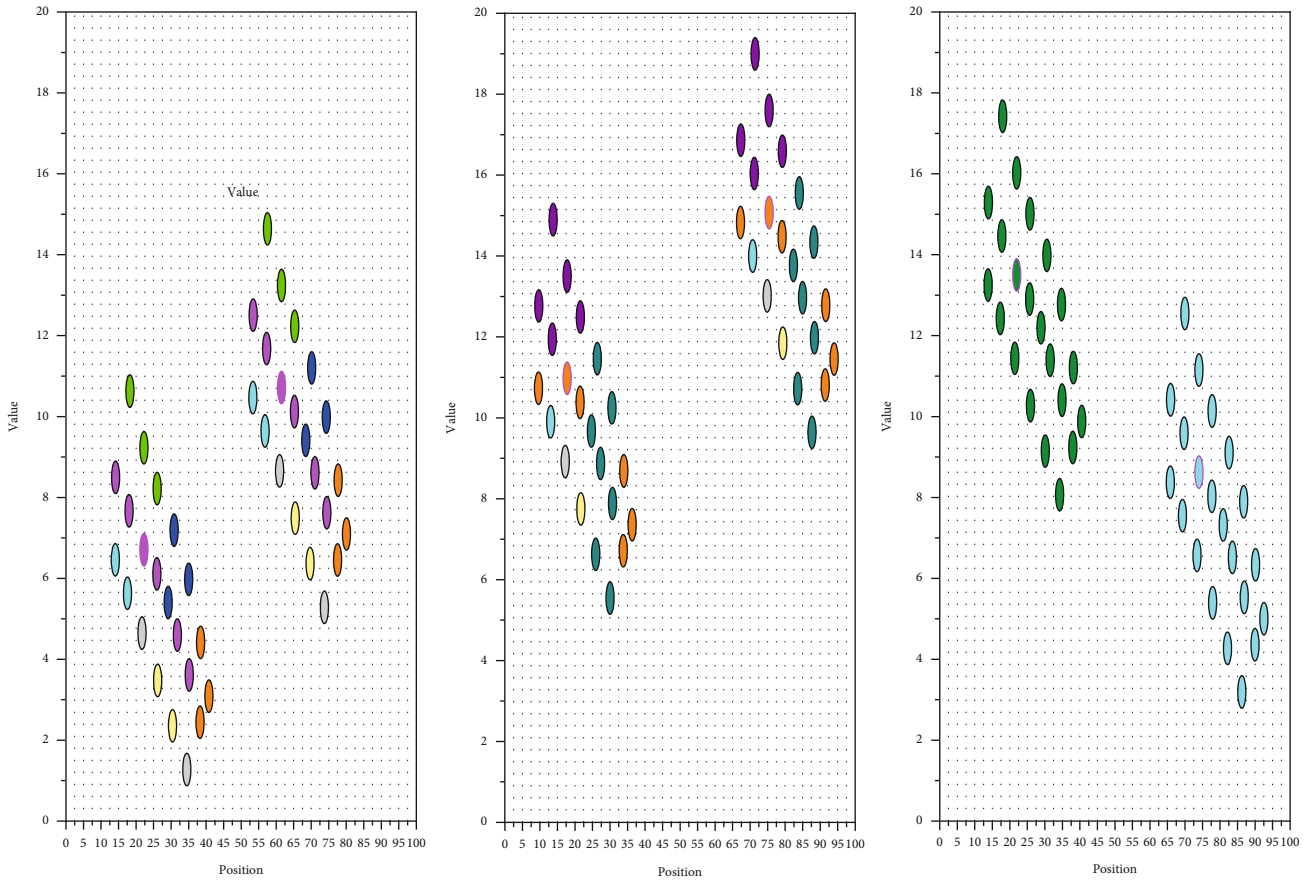

Figure 1: Coscattering point channel set for the overdetection single-point model.

utilization in transmission detection engineering, and ensures the redundancy of seismic wave imaging in the in-plane detection:

$$u(t+\Delta t) = s\sum_{m=2}^{2M}\frac{\nabla t}{k!}\frac{\partial k}{\partial t}u(t). \tag{3}$$

To resolve geological anomalies on one side of the working face roadway or other explored roadway in the direction of the following layer, multiwave imaging of one side area is performed using scattered waves. It should be noted that the mapping of the channel set is limited by two parameters, namely, travel time and spatial path, and the corresponding polarization filtering function is also changed with these two parameters; specifically for a scattering point, the travel time and path of the scattering wave are dynamic and known at the time of mapping, then the corresponding polarization factor and directional filtering factor for any sampling point signal in the records of different gun inspection pairs [16]. The directional filter factors are all dynamically obtainable. In this way, the vector wavefield separation process is completed for a specific type and region of scattered waves:

$$\rho\frac{\partial V_x^X}{\partial t} - d(x)V_x^X = \frac{\partial \sigma_{xx}}{\partial x}, \tag{4}$$

$$\rho\frac{\partial V_x^Z}{\partial t} + d(x)V_x^Z = \frac{\partial \sigma_{xx}}{\partial x}. \tag{5}$$

In the ideal field of seismic data acquisition, it is required to acquire regular and dense high-quality raw data without exceeding the project cost; however, the data acquisition is often affected by various factors, and the seismic trace data are often missing. To effectively recover the missing seismic traces, this paper proposes a high-precision seismic data reconstruction method to obtain regular and complete pre-stack seismic data, which provides an excellent data environment for subsequent data interpretation and final judgment. This paper presents an in-depth study of the data reconstruction aspects and analyzes the critical steps that affect the reconstruction effect.

As shown in Figure 2, some longitudinal and transverse lines are arranged on the ground in the vibration zone, a geophone is placed on them, and the reflected wave superimposed signals of each stratigraphic subinterface in the ground received by the geophone are sampled once every time after the source explosion, and finally, the sampled data are brought back and filtered, corrected, antifolded, etc., which finally form the longitudinal line (also called the main line), transverse line (also called contact line), and time axis line data, and are stored in Seg-Y format.

The purpose of classifying bulk data by data values is to correctly assign different color and transparency values to

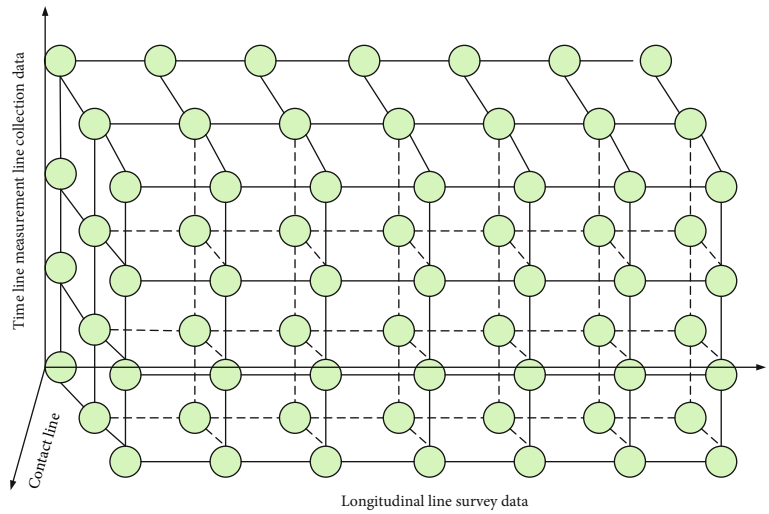

Figure 2: Logical distribution of data in 3D space.

different classes of data to correctly represent the different distributions of multiple substances or the different properties of a single substance. To achieve this, it is necessary to map the different classifications to different colors and opacities using transfer functions.

However, it is often very difficult to find a suitable transfer function to classify and map the data body, and the organization is often quite complex when many different materials coexist. For example, for seismic data, rocks of the same lithology often have different gray values depending on the layer depth, and pixels of the same gray value may belong to rocks of different lithology [17], to correctly represent the different distributions of multiple substances or the different properties of a single substance. Therefore, this problem is still an urgent research problem in the 3D visualization technology of body data. At present, for 3D data bodies with simple material composition, the two most used methods are the threshold classification method and the probabilistic classification method, and the following is a brief description of the classification of seismic body data using the threshold method.

4. Low Signal-to-Noise Ratio 3D Seismic Data Processing Design

In the analysis of time-varying signals with frequency variations over time, time-frequency analysis can represent the one-dimensional signal on a two-dimensional coordinate map with time and frequency as the horizontal and vertical coordinates, which can clearly show the time-frequency characteristics of the signal and reflect some useful information needed in signal processing. The high resolution of time-frequency representation is of great significance to the description of geological formations, and time-frequency analysis is closely related to the study of stratigraphic structure, sedimentary properties, and reservoirs.

From the theory of absorption and attenuation of seismic waves, it is known that the fluctuation equation satisfied by the displacement vector in a viscoelastic medium without physical force when seismic waves propagate in a nonperfectly elastic rock is

$$\rho \frac{\partial^2 u}{\partial t^2} = \frac{(\lambda - \mu)\nabla \mathrm{divu} + \left(\lambda' - \mu'\right)\nabla \mathrm{divu}}{\partial t} - \mu^2 \frac{\partial u}{\partial t}. \quad (6)$$

In the traditional seismic prestack data set, the first two types of tracts are generally used, the reflected wave holography is hyperbolic, and the refracted and direct wave homography is linear, with different dip angles of homography superimposed on each other, damaging the effective wave information. The signal structure is simple, and the combination of the data body before stacking with the curvilinear wave transform with scale, direction, and curvilinear singularity will theoretically achieve a more satisfactory reconstruction effect.

To further compare the different effects between the three threshold parameter formulas, first set the maximum number of iterations to 50, and draw a graph of the relationship between the number of iterations and the signal-to-noise ratio, as shown in Figure 3. To achieve this, it is necessary to map the different categories to different colors and opacities through a transfer function. From Figure 3, we can see that when the signal-to-noise ratio of 15 dB needs to be achieved, the linear threshold parameter cannot be achieved within 50 iterations, and the exponential threshold parameter needs about 27 iterations to be achieved, while the new exponential threshold parameter applied in this chapter can be completed in only 18 iterations, and the convergence speed is much faster.

In other words, the signal-to-noise ratio of the new exponential threshold parameter is higher for the same number of design iterations, and the new exponential threshold parameter is more advantageous for industrial production considerations:

$$\rho \frac{\partial^2 \varphi}{\partial t^2} = \frac{\mu' \nabla \mathrm{divu}}{\partial t} + \mu^2 \frac{\partial u}{\partial t}. \quad (7)$$

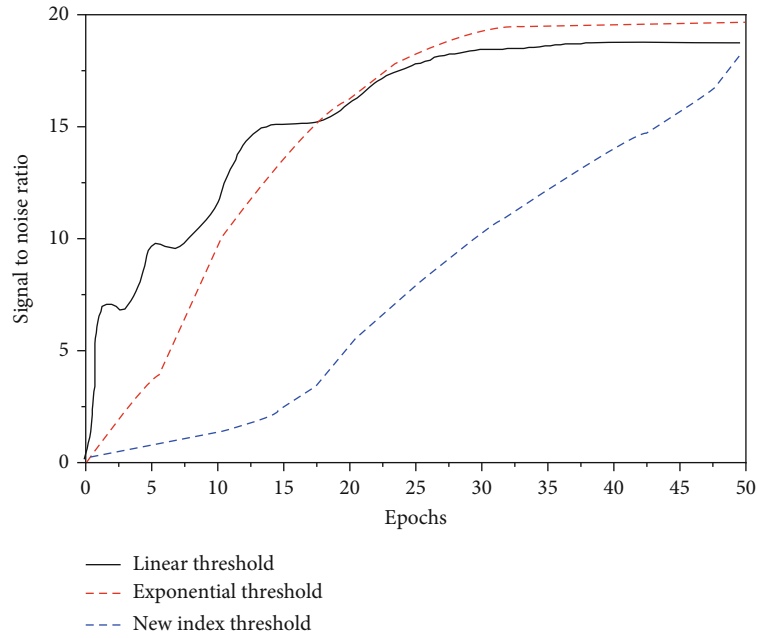

Figure 3: Number of iterations versus signal-to-noise ratio graph.

In this paper, to improve the reconstruction accuracy, the complex-valued curvilinear transform is used, but there is still a certain shortage for the computation time aspect. For this reason, this paper proposes a reconstruction method based on the frequency-domain complex-valued curvilinear transform, i.e., the Fourier transform is used first to transform the reconstruction data from the time domain to the frequency domain, and then, the reconstruction is carried out using the algorithm of this paper. Since the reconstruction data are sparse by Fourier transform before the reconstruction by curvilinear transform, the low energy effective wave coefficients are not filtered out when the convex set projection algorithm is applied, so that the in-phase axes containing high and low energy amplitudes can be reconstructed simultaneously, which is more effective than the previous reconstruction by curvilinear transform alone [18].

Moreover, since the complex-valued curvilinear transform is used, the computation time is the same whether the reconstruction is done in the time domain or the frequency domain. Although the computation time is required for transforming the time domain to the frequency domain and conjugate valuation, it is negligible compared to the computation time of the complex-valued curvilinear transform when processing a large amount of seismic data. Moreover, the time-frequency transformation process can make the data sparser, which is more conducive to the reconstruction of seismic data in the compressed sensing framework, and theoretically, the reconstruction results will be better.

The plane wave amplitude is influenced by the geometric diffusion in addition to the stratigraphic attenuation. To eliminate the influence of geometric diffusion on plane wave amplitude, the method of measuring two samples, i.e., reference sample and rock sample, can be used in petrophysical tests. The time-domain signal is converted to the frequency domain by Fourier transform as a signal in complex form, with the real part being the amplitude spectrum and the imaginary part being the phase spectrum. In the case of ignoring the phase information, only the amplitude and frequency are considered, and the reference subwave is corrected by different Q values until it can reach a certain degree of agreement with the subwave signal at the receiving point, and this method is called the spectrum simulation method. The method loses the phase information, and although it is possible not to focus on the fit at the time point, only to compare the similarity of the corresponding frequencies, the information does bring unavoidable errors, as shown in Figure 4.

Since the mapped texture elements may not be aligned with the coordinates in the texture space where the corresponding data points are located, they need to be resampled to obtain more accurate texture values. The simplest way to handle this is to use the trilinear interpolation of the mapping results of the eight nearest data points for a sample point in the texture slice to obtain a more accurate texture value for that sample point.

The wavelet coefficients are in different scales, i.e., the representation of the original signal at multiple resolutions [19]. It can clearly show the time-frequency characteristics of the signal, reflecting some useful information needed in signal processing. It is easier to distinguish the effective signal from the random noise under multiscale decomposition by the transmission characteristics because the wavelet coefficients of the signal increase with scale while the coefficients representing the noise decrease. Thus, we can choose an appropriate threshold to extract the effective signal and smooth the noisy signal. In the near-surface loose sediment layer, the geometric seismology based on elastic wave theory is no longer fully applicable, and the dispersion characteristics possessed by the surface waves are directly related to the layered structure of the medium, which provides a basis for

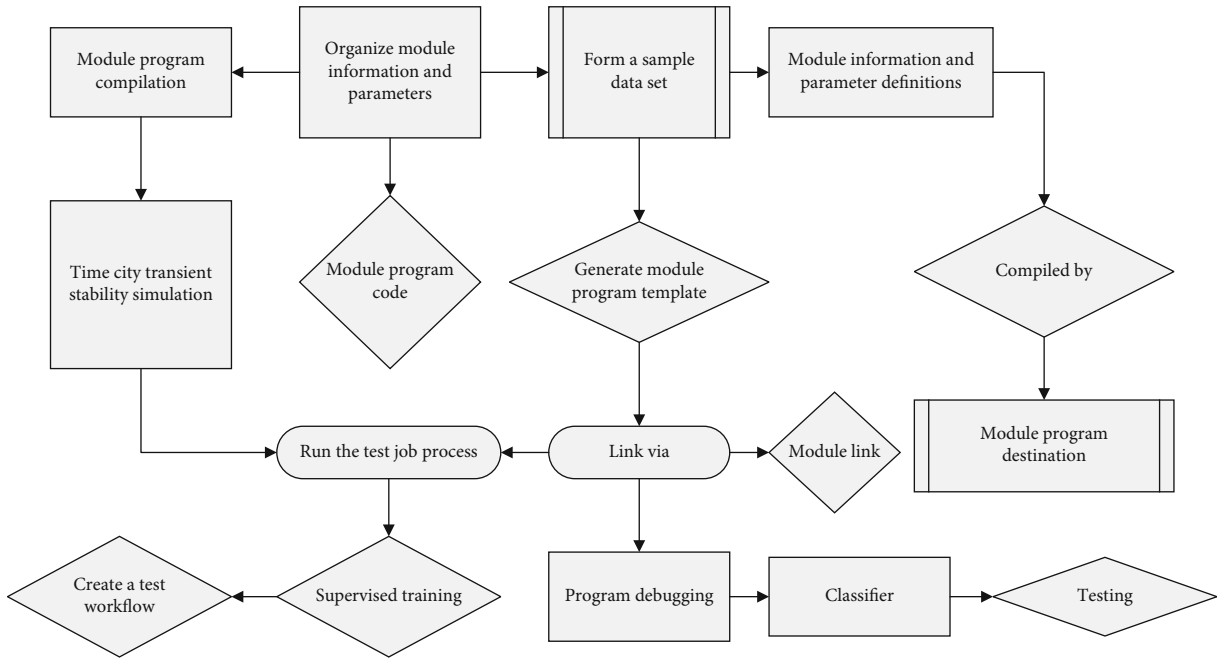

Figure 4: Processing steps.

estimating the near-surface property parameters using the surface wave dispersion characteristics.

$$f_{\max} = \frac{1}{|\partial t/\partial l|\nabla l}. \tag{8}$$

5. Experimental Design of Imaging

The offset/antioffset aperture is an important parameter in the Kirchhoff-type prestack offset/antioffset implementation technique. The size of the aperture determines the range of seismic traces that contribute to the pixels of the imaged spot. It is difficult to accurately calculate the optimal offset or counteroffset aperture during the actual calculation. Therefore, the best offset/counteroffset aperture value for imaging can be selected based on the actual processing experience, considering the burial depth, dip angle, and other factors. For a certain seismic record, the coordinates of its centerpoint can be determined, and the cone with this center point coordinate as the vertex will be used as the offset/antioffset aperture. The size of the aperture gradually increases with depth, and the size of the desired aperture can be defined by choosing the appropriate offset angle. The actual calculation process usually takes a relatively small offset angle in the vertical measurement line direction and a relatively large offset angle along the measurement line direction. The reverse offset aperture is selected as above.

There is no higher frequency component in the seismic data body than the maximum temporal frequency, which represents the maximum temporal frequency to avoid artifacts at the intersection of the trace and the operator trajectory as a function of the local operator dip and trace spacing. In order not to generate operator spurious frequencies, the sampling sequence of the summed seismic trace data superimposed along the offset/antioffset operator trajectory needs to satisfy the Nyquist sampling criterion:

Firstly, a prestack depth offset is applied to the arbitrary nonzero gun-check distance seismic data, and then, a zero gun-check distance inverse offset is applied to the offset imaging data to output the zero gun-check distance data, and the reflection coefficients can be maintained during the transformation process.

In near-surface velocity structure imaging, the first-to-wave walk-time tomography method usually produces a smooth velocity model. When there is a low-velocity weathering layer overlying the high-velocity bedrock in the near-surface structure, the first-to-wave travel time planimetric imaging method may not be able to invert the sharp boundary. However, based on the same travel time information, the refracted wave travel time offset method can accurately calculate the location of the refracted layer. The method obtains the position information of the refractive layer by downward extension of the refractive wave walk-time profile and a given overlying layer velocity. In this chapter, the joint inversion method of refractive wave travel-time offset imaging and velocity is proposed, as shown in Figure 5.

The method first calculates the position of the refractive layer by the refractive wave walk-time offset method and further constrains the first-to-wave walk-time laminar imaging inversion by transforming the refractive layer obtained from the offset into a discontinuity of the regularization term in the inversion objective function. The refractive layer position shape and velocity model obtained by the offset is updated simultaneously in each subsequent iteration. To accommodate more complex cases, the method is further extended to the multilayer medium case [20]. Although

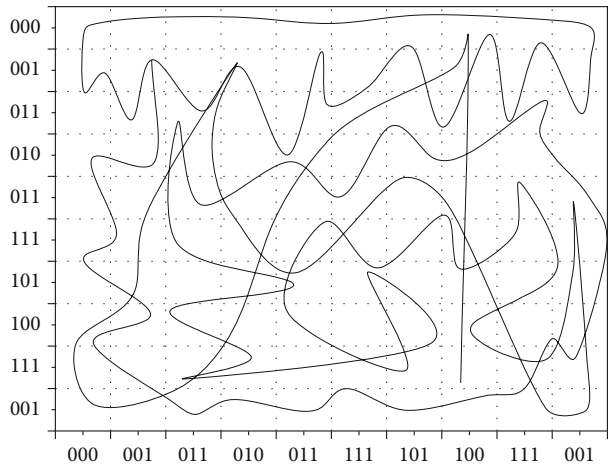

Figure 5: Third-order 3D gray curve.

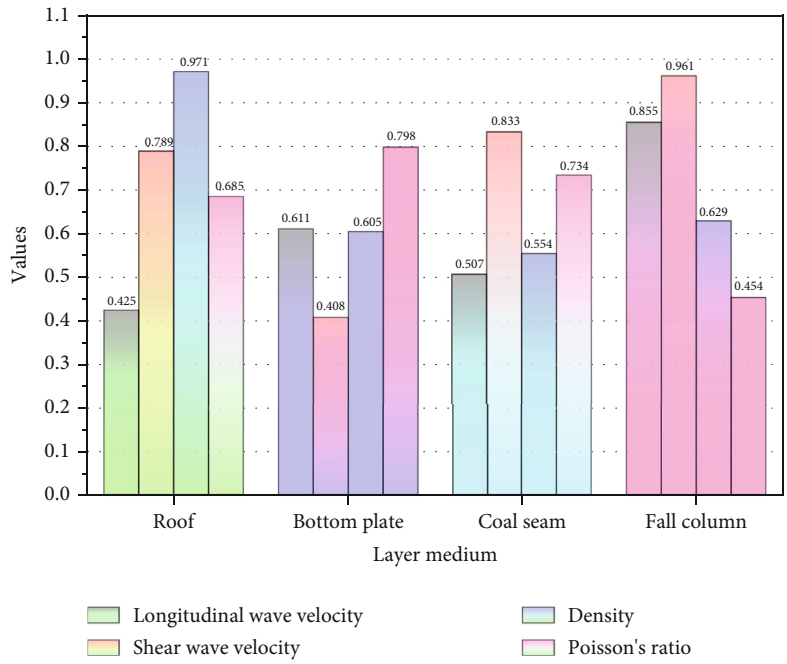

Figure 6: Parameters of the 3D model of the working surface.

transforming the time domain to the frequency domain and conjugate evaluation requires computational time, this is not the case when dealing with large amounts of seismic data. Theoretical model tests show that the joint inversion method demonstrates superiority in reconstructing near-surface models with strong velocity contrast compared to the conventional Tikhonov regularized first-to-wave walk-time laminar imaging method and the delay time method. In practical data applications, the near-surface velocity model obtained by this joint inversion method can calculate more accurate long-wavelength static correction values and make the reflection layer energy more concentrated in the superimposed profile.

When geologists continuously browse the 3D seismic data body, the data block corresponding to each frame is determined by the viewpoint coordinates and observation direction of the current frame, and the viewpoint coordinates and angle change continuously as the browsing progress, forming the viewpoint motion trajectory. Therefore, by fitting the viewpoint trajectory and predicting the viewpoint coordinates at the next moment, the potential domain data can be obtained from the predicted coordinates to realize the preloading operation of the predicted data blocks and reduce the lagging sensation during the continuous viewing of the frames, as shown in Figure 6.

The basis of the Hilbert-R tree is to map the location coordinates of data in high-dimensional space to the encoded values of the corresponding filled curves. Therefore, a stable fractal curve with high filling quality is one of the conditions to ensure the query performance of the Hilbert-R tree.

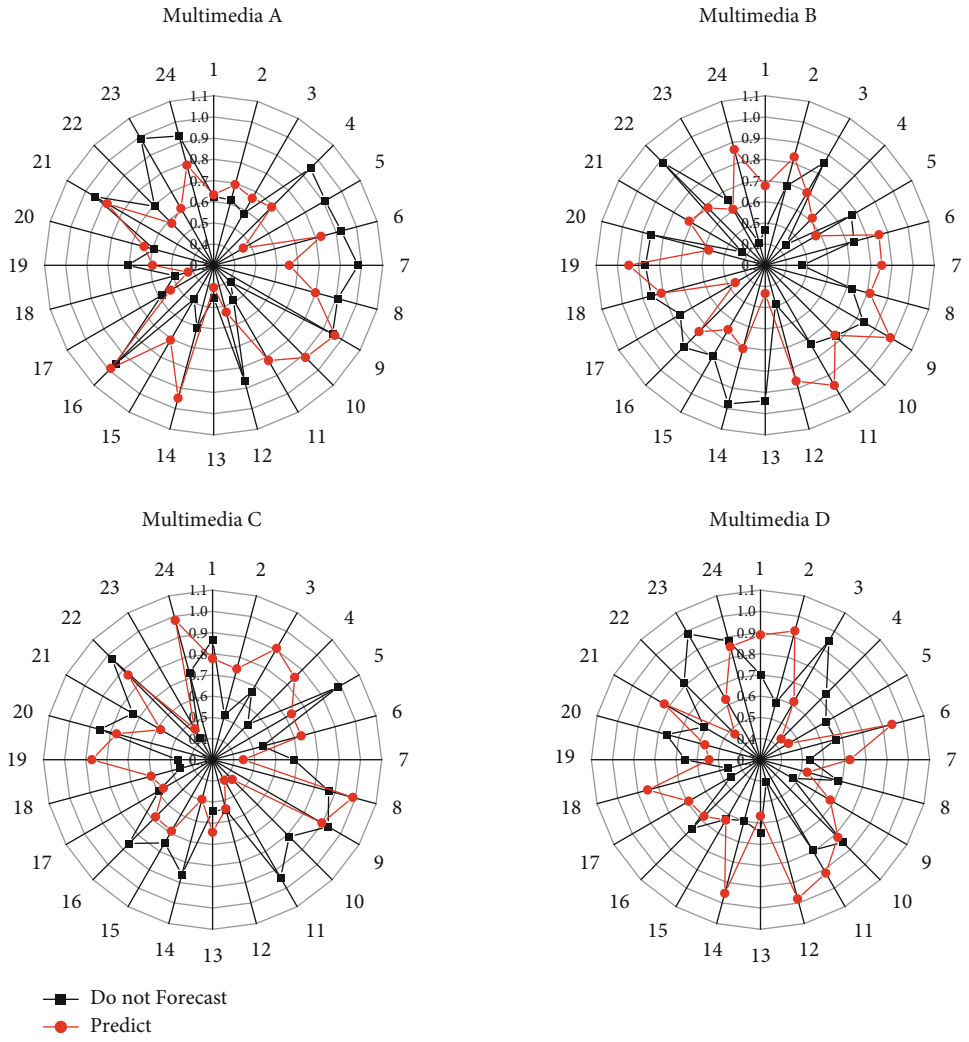

Figure 7: Efficiency comparison.

6. Analysis of Results

In the three-dimensional visualization process, excluding the rendering time, the indexing time of the target data block accounts for most of the total time consumed. In general, the query time of the node is greater than the indexing time of the target data within the node, so it can be said that the access efficiency of the node determines the time consumed by the data indexing in the display process.

This enhancement is based on the superiority of the Hilbert-*R* tree structure using clustering technology: the Hilbert-*R* tree is faster than octree, for all its nodes; except the last node at each level, the rest of the nodes are filled, i.e., for the same volume of data bodies, the number of subblocks generated by the Hilbert-*R* tree is often much less than that of the octree, so its indexing speed is higher than that constructed by the octree structure. By analyzing the different characteristics of coal seam seismic waves in the time-frequency domain and polarization parameters, the signal characteristics of the actual seismic wave field in the mine space were revealed, and the field applicability of the two types of geophones was evaluated. The Hilbert-*R* tree based on cure clustering, based on the Hilbert-*R* tree, performs clustering operations on data bodies in advance to ensure that the Hilbert code values of adjacent MBC centroids

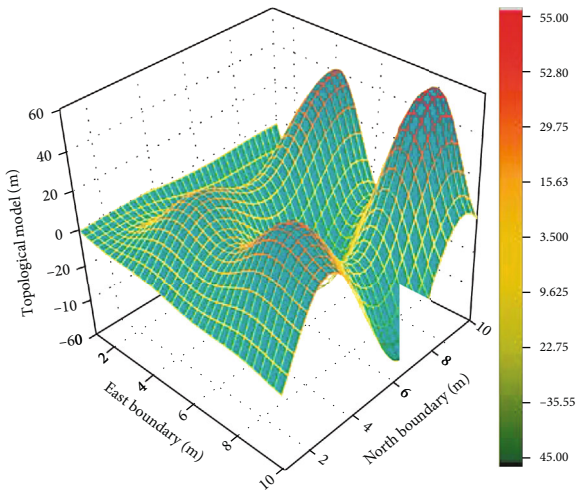

Figure 8: Sounding vibration effect.

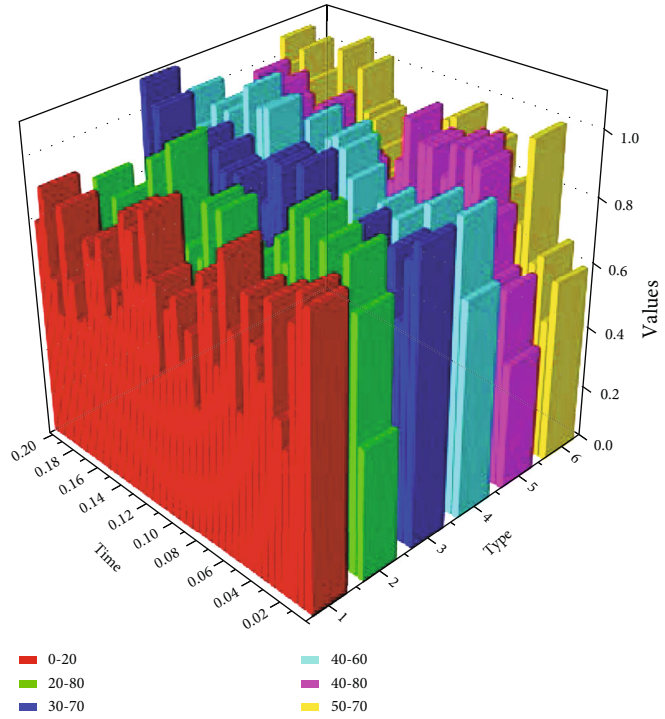

Figure 9: Estimated Q values for different fitted bands.

generated at the end are also similar, i.e., for data adjacent to each other in the spatial structure, their storage locations are also similar, thus effectively reducing the number of disk accesses and thus improving indexing efficiency.

To ensure that the 3D visualization of large-scale seismic data will not be stalled or stuttered, it is necessary to keep the frame rate of the rendering at 24 fps or more. The average frame rate was recorded and compared with the frame rate without prediction, and the results are shown in Figure 7.

The proposed preloading method based on viewpoint motion prediction not only has a high frame rate for visualization of data A and B with small data volume but also maintains a frame rate of about 24 fps for data body C with a size of 10 GB. Compared with the method without preloading, the frame rate increases by 3.2%~46.54% as the data volume increases.

For strong surface waves, low-frequency chirp vibration, wild value interference, and low-frequency strong energy interference, the adaptive coherent noise attenuation technology with high fidelity and split-frequency high-energy noise suppression technology are selected to effectively suppress them. Amplitude preserving noise suppression needs to meet the requirements of maintaining the relative amplitude, waveform, frequency, and phase and suppression filtering as far as possible to meet the requirements of zero phase, amplitude all-pass, and denoising process specifically using four methods to evaluate the denoising effect. The effective signal cannot exist in the suppressed noise. Before and after the suppression, the spectrum can only show the frequency range of the noise. In the single-frequency noise suppression process, the effective signal of the same frequency band cannot be damaged. After the noise suppression, the relative relationship between the effective signal amplitude and energy remains unchanged, and no false frequency phenomenon occurs.

Due to the wide frequency band of the surface wave, the use of an adaptive coherent noise attenuation technique will cause the phenomenon of false frequency; the treatment of the surface wave for the low-frequency band and the high-frequency band of two frequency bands was repeatedly suppressed to maximize the fidelity of the denoising. The collected seismic signals contain random noise and regular noise. The low-frequency chirp developed in the work area is attenuated using the adaptive coherent noise attenuation technique and the predictive antifold technique. The spectrum analysis before and after the chirp suppression in Figure 8 shows that not only the chirp is successfully suppressed but also the effective wave energy is not hurt, and the relative fidelity is achieved in the process of suppressing the surface wave.

The use of split-frequency high-energy noise suppression technology attenuates wild-value interference and strong energy interference in each frequency band. Because the abnormal amplitude energy difference between low and high frequency is large, the low-frequency effective signal may also be mixed with the high-frequency noise signal; wanting to eliminate noise at the same time to protect the effective signal needs to be divided into frequency noise attenuation. The split-frequency high-energy noise suppression technique is to calculate the weighting curve based on the numerical relationship between noise and signal in different frequency bands, perform noise reduction, and then reconstruct the seismic record.

Through fine spherical diffusion and two surfaces' consistent amplitude compensation, the amplitude attenuation caused by the absorption of frequency by the earth is eliminated. It is ensured that the splicing energy of different

blocks of data is consistent, and the relative amplitude curves of the conventional processing profiles and the high-fidelity processing profiles are compared, and the high-fidelity processing maintains the amplitude properties of the data better. Not only the resolution and fidelity are required to be guaranteed but also the processing efficiency needs to be greatly improved to adapt to the complexity and difficulty of exploration work. In the application process, the relative strength and weakness of the amplitude are not artificially changed, and the amplitude can objectively and effectively reflect the subsurface geological interface information and achieve amplitude fidelity as much as possible.

It is generally believed that once the extracted subways are correct, the folded processing will preserve the amplitude, but the extraction of subwaves is affected by various factors such as noise, so the folded processing can only preserve the amplitude relatively, and the good control technology is used to judge the fidelity effect in the process of improving the resolution. The error between the seismic data and the actual well data is gradually reduced so that each step of the resolution improvement process for the Shawan Formation can be based on evidence, and relative fidelity is achieved in the process of resolution improvement, as shown in Figure 9.

The Q value estimation accuracy is the highest and most stable in the frequency range of 40-60 Hz, and the absolute error of Q value estimation is about 2%. The reason is that 40-60 Hz is the closest to the main frequency of seismic subwaves, and the frequency band concentrates the main energy of seismic waves. 0-120 Hz range has the highest estimation error, and the error becomes larger as the seismic wave propagation time increases, and the amplitude decreases as the seismic wave propagates to the deeper part of the ground due to the energy attenuation caused by the absorption and attenuation of the ground, and there is also the effect of the pickup error of the first-to-wave time.

Comparing the estimation results in two different frequency bands, 30-70 Hz and 50-70 Hz, we can see that the estimation results in 30-70 Hz are more stable, indicating that the seismic wave absorption and attenuation in the low-frequency band are lower than the seismic wave absorption and attenuation in the high-frequency band, and the analysis results are consistent with the seismic wave absorption and attenuation theory in which the attenuation of high-frequency seismic waves is stronger. Only the upgoing waves from the subsurface can be received; in the vertical seismic section, because the geophone is placed inside the formation through the well, it can receive both the upgoing waves propagating from the bottom up and the upgoing waves propagating from the top down. Therefore, when estimating Q values using actual seismic data, a reasonable fitting band should be selected within the effective frequency bands of different data, which can effectively avoid the errors caused by noise interference.

7. Conclusion

The equivalent offset distance scattered wave imaging method has good scattered wave extraction capability with a high superposition number and low signal-to-noise ratio requirement. The adaptive instantaneous polarization parameter acquisition method based on the Hilbert transform with a time window can dynamically acquire accurate polarization parameters for each sampling point signal, and the dynamic polarization filtering function can be established by combining with the typical seismic wave polarization characteristics of the mine. The polarization filter function is invalid for conversion waves with the same type of polarization characteristics, and the relevant interference waves can be eliminated by the conversion wave velocity difference that can be designed as a suppression factor. In the roadway overdetection, the original observation system can be changed to expand the offset distance by establishing an equivalent virtual survey line perpendicular to the roadway direction; in the workforce transmission wave observation, the scattered wave travel time of different depth scattering points under the concept of two-dimensional equivalent offset distance does not satisfy the hyperbolic relationship, and the purpose of using the scattered wave signal in the transmission record cannot be reached, while the three-dimensional equivalent offset distance method in the workforce can extend the detection direction. The method can extend the detection direction to the depth direction of the top and bottom plates of the working face, to carry out the scattered wave imaging of the top and bottom plates. It is more helpful to reveal the inherent laws of geoscience data, to carry out activities such as energy detection, and then generate huge economic benefits. In the roadway overdetection, the original observation system can be changed, and the offset distance can be expanded by establishing an equivalent virtual survey line perpendicular to the roadway direction; in the workforce transmission wave observation, the scattered wave travel time of different depth scattering points under the concept of two-dimensional equivalent offset distance does not satisfy the hyperbolic relationship, and the purpose of using the scattered wave signal in the transmission record cannot be achieved, while the workforce three-dimensional equivalent offset distance method can extend the detection. The 3D equivalent offset distance method of the working face can extend the detection direction to the depth direction of the top and bottom of the working face, to carry out the scattered wave imaging of the top and bottom of the working face.

Data Availability

No data were used to support this study.

Conflicts of Interest

The authors declare that there is no conflict of interest with any financial organizations regarding the material reported in this manuscript.

References

[1] D. Liu, W. Wang, X. Wang, C. Wang, J. Pei, and W. Chen, "Poststack seismic data denoising based on 3-D convolutional

neural network," *IEEE Transactions on Geoscience and Remote Sensing*, vol. 58, no. 3, pp. 1598–1629, 2020.

[2] M. Waage, S. Bünz, M. Landrø, A. Plaza-Faverola, and K. A. Waghorn, "Repeatability of high-resolution 3D seismic data," *Geophysics*, vol. 84, no. 1, pp. B75–B94, 2019.

[3] S. Yuan, S. Wang, C. Luo, and T. Wang, "Inversion-based 3-D seismic denoising for exploring spatial edges and spatio-temporal signal redundancy," *IEEE Geoscience and Remote Sensing Letters*, vol. 15, no. 11, pp. 1682–1686, 2018.

[4] N. Lebedeva-Ivanova, S. Polteau, B. Bellwald, S. Planke, C. Berndt, and H. H. Stokke, "Toward one-meter resolution in 3D seismic," *The Leading Edge*, vol. 37, no. 11, pp. 818–828, 2018.

[5] N. Salaun, H. Toubiana, J. B. Mitschler et al., "High-resolution 3D seismic imaging and refined velocity model building improve the image of a deep geothermal reservoir in the Upper Rhine Graben," *The Leading Edge*, vol. 39, no. 12, pp. 857–863, 2020.

[6] H. Karbalaali, A. Javaherian, S. Dahlke, R. Reisenhofer, and S. Torabi, "Seismic channel edge detection using 3D shearlets—a study on synthetic and real channelised 3D seismic data," *Geophysical Prospecting*, vol. 66, no. 7, pp. 1272–1289, 2018.

[7] A. Malehmir, A. Tryggvason, C. Wijns et al., "Why 3D seismic data are an asset for exploration and mine planning? Velocity tomography of weakness zones in the Kevitsa Ni-Cu-PGE mine, northern Finland," *Geophysics*, vol. 83, no. 2, pp. B33–B46, 2018.

[8] M. Protasov, V. A. Tcheverda, and A. P. Pravduhin, "3D true-amplitude anisotropic elastic Gaussian beam depth migration of 3D irregular data," *Journal of Seismic Exploration*, vol. 28, no. 2, pp. 121–146, 2019.

[9] A. Bakulin, P. Golikov, M. Dmitriev, D. Neklyudov, P. Leger, and V. Dolgov, "Application of supergrouping to enhance 3D prestack seismic data from a desert environment," *The Leading Edge*, vol. 37, no. 3, pp. 200–207, 2018.

[10] K. Shiraishi, G. F. Moore, Y. Yamada, M. Kinoshita, Y. Sanada, and G. Kimura, "Seismogenic zone structures revealed by improved 3-D seismic images in the Nankai Trough off Kumano," *Geochemistry, Geophysics, Geosystems*, vol. 20, no. 5, pp. 2252–2271, 2019.

[11] A. Schaaf and C. E. Bond, "Quantification of uncertainty in 3-D seismic interpretation: implications for deterministic and stochastic geomodeling and machine learning," *Solid earth*, vol. 10, no. 4, pp. 1049–1061, 2019.

[12] S. Cordery, "An effective data processing workflow for broadband single-sensor single-source land seismic data," *The Leading Edge*, vol. 39, no. 6, pp. 401–410, 2020.

[13] H. Wang, W. Chen, W. Huang et al., "Nonstationary predictive filtering for seismic random noise suppression—a tutorial," *Geophysics*, vol. 86, no. 3, pp. W21–W30, 2021.

[14] G. Bellefleur, S. Cheraghi, and A. Malehmir, "Reprocessing legacy three-dimensional seismic data from the Halfmile Lake and Brunswick No. 6 volcanogenic massive sulphide deposits, New Brunswick, Canada," *Canadian Journal of Earth Sciences*, vol. 56, no. 5, pp. 569–583, 2019.

[15] Z. Wang, H. Di, M. A. Shafiq, Y. Alaudah, and G. AlRegib, "Successful leveraging of image processing and machine learning in seismic structural interpretation: a review," *The Leading Edge*, vol. 37, no. 6, pp. 451–461, 2018.

[16] A. El-Emam, M. Al-Otaibi, and C. Koeninger, "Workshop explores advances in land seismic data processing," *The Leading Edge*, vol. 38, no. 12, pp. 960–965, 2019.

[17] M. Mohammadi, B. Soleimani, and M. Mahmoudian, "Predicting abnormal formation pressure using 3D seismic velocity, in Kupal Oil Field," *Journal of Petroleum Research*, vol. 27, no. 96-6, pp. 103–115, 2018.

[18] H. Cheng, K. Xie, C. Wen, and J. B. He, "Fast visualization of 3D massive data based on improved Hilbert R-tree and stacked LSTM models," *IEEE Access*, vol. 9, pp. 16266–16278, 2021.

[19] A. Malehmir, M. Markovic, P. Marsden et al., "Sparse 3D reflection seismic survey for deep-targeting iron oxide deposits and their host rocks, Ludvika Mines, Sweden," *Solid Earth*, vol. 12, no. 2, pp. 483–502, 2021.

[20] Y. Chen, "Fast dictionary learning for noise attenuation of multidimensional seismic data," *Geophysical Journal International*, vol. 222, no. 3, pp. 1717–1727, 2020.